Time sequential prediction of ventricular-vascular interactions

TERRY W. LATSON, WILLIAM C. HUNTER, DANIEL BURKHOFF, AND KIICHI SAGAWA
Departments of Anesthesiology and Biomedical Engineering, School of Medicine, The Johns Hopkins University, Baltimore, Maryland 21205

LATSON, TERRY W., WILLIAM C. HUNTER, DANIEL BURKHOFF, AND KIICHI SAGAWA. *Time sequential prediction of ventricular-vascular interactions.* Am. J. Physiol. 251 (Heart Circ. Physiol. 20): H1341–H1353, 1986.—A new analytical method (sequential convolution) for describing ventricular-vascular interactions was used to predict instantaneous pressure and flow in four isolated canine left ventricles ejecting into a computer-simulated arterial system. Ventricular pumping ability was described by a load-independent elastance, [$E^*(t)$] combined with a ventricular internal resistance. "Arterial" properties were characterized using a time-based impulse response function that is derived from impedance measurements. Sequential convolution was then used to couple these independent descriptions of ventricular and vascular properties. Predicted pressure-volume trajectories, as well as instantaneous pressures and flows, closely matched the experimental data. Stroke volume, peak pressure, and peak flow were typically within 5% of measured values. This method provides a powerful analytical technique for examining ventricular-vascular interactions and has potential application in evaluating the ventricular-loading effects of more complex in vivo vascular properties.

isolated canine heart; ventricular pressure-volume ratio; ventricular internal resistance; vascular impedance; vascular impulse response; sequential convolution

---

THE HEART AND VESSELS form a coupled system in which the properties of both components interact to determine resultant pressures and flows. Prediction of these pressures and flows and how they will be altered by changes in ventricular and/or vascular properties require *1*) independent descriptions of ventricular and vascular properties, and *2*) a means of coupling these descriptions to predict the consequences of their interaction. This paper describes a new method (sequential convolution) by which this latter step may be achieved. In contrast to previous work, this new method predicts the entire time course of flow and pressure (not just mean pressure and stroke volume), can incorporate flow-dependent ventricular properties, and is not (in principle) restricted to lumped finite-element descriptions of the arterial load.

As recently elaborated by Campbell et al. (3), the interaction between the left ventricle (LV) and systemic arterial system may be thought of as a feedback loop involving ventricular outflow and aortic pressure. Ventricular outflow into the arterial system produces an aortic root pressure, which in turn feeds back onto the LV to determine LV outflow. Both prior flow and instantaneous flow combine with arterial properties to determine this feedback pressure.

The sequential convolution method correspondingly involves describing this feedback pressure developed at the aortic root as consisting of two parts. The first component may be thought of as pressure that is caused by all prior flow into the vascular system. For example, in the real arterial system this prior flow is what gave rise to vascular reflections that may now be returning to the aortic root. For Windkessel models of the arterial system, this prior flow is what determines the present volume and pressure inside the Windkessel. The second component of the aortic feedback pressure is the instantaneous pressure generated by flow existing at the present instant. The time-varying ventricular pressure-volume relationship then describes how the ventricle interacts with these developed pressures in terms of resultant changes in systolic ventricular volumes.

The purpose of the present study was to predict the time course of ventricular pressure, ventricular volume, and aortic pressure resulting from ventriculoarterial interactions by coupling independent descriptions of ventricular and vascular properties. As an initial test of this method we obtained data from real ventricles ejecting into a computer-simulated Windkessel model of the arterial system. In our analysis, ventricular mechanical performance is characterized by ventricular elastance (i.e., the time-varying ratio of ventricular pressure to ventricular volume) and by ventricular internal resistance. "Vascular" properties are described using impulse-response methods, which are the time-based counterpart of frequency-based impedance methods. These independent time-based expressions of ventricular and vascular properties are then analytically coupled by the process of sequential convolution discussed above. We validated these predicted pressures and volumes against measured data obtained over a wide range of afterload conditions.

Abbreviations

C	Parallel capacitance of three-element Windkessel
$E^*(t)$	Estimated isovolumic ventricular elastance
E^*_{max}	Maximum value of $E^*(t)$
$F(t)$	Ventricular flow
ITR	Impulse train response

$P(t)$	Ventricular pressure
$P_A(t)$	Simulated arterial pressure
$P_I(t)$	Estimated isovolumic ventricular pressure
R	Ventricular internal resistance
R_c	Series resistance of three-element Windkessel
R_p	Parallel resistance of three-element Windkessel
RF	Resistance factor (used to describe R)
SIR	Single impulse response
t^*_{max}	Time of maximal $E^*(t)$
V^*_d	Volume axis intercept for $E^*(t)$ function
$V(t)$	Ventricular volume

MATERIALS AND METHODS

Experimental Preparation

Both the surgical preparation and experimental apparatus have been described in detail elsewhere (27, 28); only a brief summary is given here. Following induction of anesthesia with pentobarbital sodium (30 mg/kg), the heart of an ~20-kg mongrel dog is excised and connected to a volume-control servo pump. The isolated heart is supported by cross circulation with another pentobarbital-anesthetized dog. Blood from the support dog, after passing through a heat exchanger, is pumped into the excised aortic root under constant pressure of 100 mmHg. Blood is returned to the support dog via a drainage chamber collecting blood from right and left ventricular vents.

To hydraulically couple the left ventricle to the volume-control servo pump, the mitral valve is excised and a retaining plate is sutured into the valve ring. A thin latex balloon is then fitted into the left ventricular cavity. This balloon is mounted on a short tubelike adapter that can be secured to the retaining plate at one end and attached to the volume-control servo pump at the other end. Ventricular pressure is measured via a catheter-tip micromanometer passed through the tube adaptor into the ventricular cavity.

Ventricular pressure is used as the input to a microprocessor that compares the instantaneously developed ventricular pressure to simulated aortic pressure. This later is determined by the microprocessor based on the prior history of ventricular ejection and the designated arterial parameters (series resistance, R_c; parallel resistance, R_p; and parallel capacitance, C). When systolic ventricular pressure begins to excede simulated aortic pressure, the microprocessor adjusts ventricular volume in a manner to simulate ejection into the three-element Windkessel loading system. Both the Windkessel parameters and ventricular diastolic filling can be adjusted at the computer terminal.

Data used in the present analysis consisted of left ventricular pressure, left ventricular volume, and simulated aortic pressure. Analog signals were digitized at a rate of 200 samples/s and stored on magnetic tape. Subsequent calculations were performed on an IBM personal computer.

Analytical Methods

Ventricular property identification. Ventricular properties were described by the combination of a time-varying ventricular elastance $E(t)$ in series with a ventricular internal resistance $R(t)$. Ideally, $E(t)$ describes the ratio of instantaneous ventricular pressure $P(t)$ and volume $V(t)$, being conventionally defined as

$$E(t) = P(t)/[V(t) - V_d]$$

where V_d is the volume axis intercept constructed from several pressure-volume loops (23, 25). However, when this description is applied to ejecting hearts, the $E(t)$ measurements obtained exhibit a certain amount of variability with loading conditions due to the reduced ability of the LV to generate pressure while it is also generating flow. $R(t)$ is a variable pressure-dependent resistance that can be used to account for these flow-related pressure reductions (8, 17, 18, 24). By combining these two descriptions of ventricular properties, we derived a flow-independent expression for ventricular pumping ability, to be denoted $E^*(t)$.

To maintain potential applicability to in vivo studies, we limited our analysis to data from ejecting beats only. To account for the effects of ventricular internal resistance, the measured pressure during ejection, $P(t)$, was related to a corresponding flow-corrected pressure, $P_I(t)$, by the following equation

$$P_I(t) = P(t) + [F(t) \times R(t)] \quad (1)$$

where $F(t)$ is measured ejection flow. $P_I(t)$ is an estimate of the pressure that would have been present if there were no flow-related (i.e., resistive) effects. Stated another way, $P_I(t)$ is an estimate of the pressure that would have existed at this same time after onset of systole if the ventricle had contracted isovolumically with the same volume that was in the ventricle at this instant [i.e., the volume given by $V(t)$ at time = t].

Although some investigators have used a constant value for $R(t)$ (4, 6), direct measurements have indicated that this internal resistance has a variable magnitude that is proportional to isovolumic pressure (8, 17, 18). The concept of a variable pressure-dependent resistance is also consistent with inverse force-velocity relationships described in isolated cardiac muscle studies (14, 20). In the present experiments, this time-variant pressure-dependent resistance is described by

$$R(t) = P_I(t) \times RF \quad (2)$$

where RF is a constant called the resistance factor. RF may be thought of as a proportionality factor relating ventricular internal resistance to instantaneous ventricular pressure. Combining *Eqs. 1* and *2* now gives

$$P_I(t) = P(t) + \{F(t) \times [P_I(t) \times RF]\} \quad (3)$$

or rearranging gives

$$P_I(t) = P(t)/(1 - [F(t) \times RF]) \quad (4)$$

Based on the results of prior studies using the isolated canine left ventricle, an assumed value of 0.0015 s/ml was used for RF (8, 17, 18, 24).

The flow-corrected pressure $P_I(t)$ (from *Eq. 4*) may now be used in the ventricular elastance function. The resulting elastance description, $E^*(t)$, has the same form

as the usual expression of $E(t)$

$$E^*(t) = P_I(t)/[V(t) - V_d^*] \quad (5)$$

where $V(t)$ is instantaneous ventricular volume and V_d^* is the volume-axis intercept for the $E^*(t)$ model. By combining *Eqs. 4* and *5*, $E^*(t)$ may be expressed in terms of the measured ejecting pressure $P(t)$

$$E^*(t) = \frac{P(t)/(1 - [F(t) \times RF])}{V(t) - V_d^*} \quad (6)$$

A single $E^*(t)$ curve to characterize each ventricle was determined as follows: data were collected over a wide range of loading conditions during periods of presumed constant contractility. For example, the pressure-volume trajectories measured from *ventricle 3* are shown in Fig. 1*A*. Using *Eq. 4*, $P_I(t)$ was calculated from the measured variables $P(t)$ and $V(t)$ [where $F(t) = -dV(t)/dt$]. Pressure-volume trajectories of $P_I(t)$ versus $V(t)$ were then constructed, as shown in Fig. 1*B*.

V_d^* was calculated from a least-squares fit regression line drawn through the points of maximal elastance. To localize these maximal elastance points, zero was used as an initial estimate of V_d^* in the equation of $E^*(t)$. Thus using *Eq. 6* with $V_d^* = 0$, the time of the maximal value of $E^*(t)$ for each $P_I(t)$ versus $V(t)$ loop is determined. A regression line is then constructed through these points. The volume-axis intercept of this line provides a new estimate of V_d^*. This new estimate of V_d^* is now used in *Eq. 6*, the times of maximal $E^*(t)$ again computed, and a new regression line drawn through these points. This process is continued until a stable value for V_d^* is obtained.

Figure 2*A* depicts the resultant $E^*(t)$ curves corresponding to the $P_I(t)$ versus $V(t)$ loops in Fig. 1*B*. All 15 curves were obtained from *ventricle 3*. Twelve of these curves essentially superimpose up to the time of maximal $E^*(t)$. More than 90% of ventricular ejection usually occurs during this rising phase of the $E^*(t)$ curve. Over this same time frame, the remaining three curves show only small deviations from these 12. These $E^*(t)$ curves

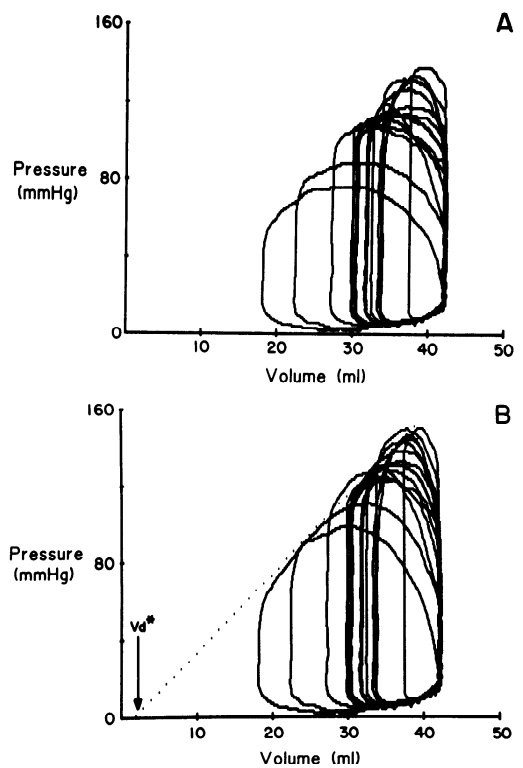

FIG. 1. Pressure-volume loops for *ventricle 3*. *A*: recorded pressure-volume data for 15 different loading conditions. *B*: corresponding $P_I(t)$ volume loops and calculated regression line through points of maximal elastance. V_d^* is intercept of this line with volume axis (see text and ABBREVIATIONS for details).

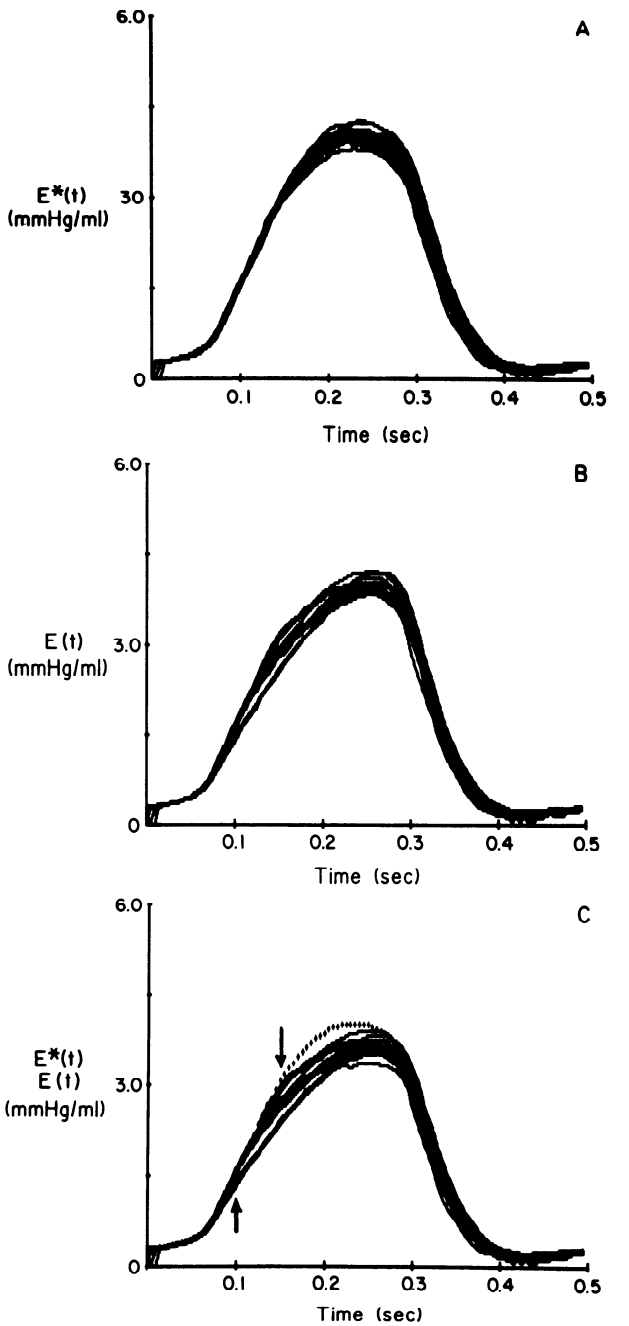

FIG. 2. Elastance curves derived from data of Fig. 1. *A*: $E^*(t)$ curves calculated from $P_I(t)$ and $V(t)$ for 15 different loading conditions. *B*: $E(t)$ curves calculated from $P(t)$ and $V(t)$. *C*: average $E^*(t)$ curve from *A* (*dotted line*) compared with $E(t)$ curves; $E(t)$ curves fall below the $E^*(t)$ curve beginning with onset of ejection (2 *arrows* mark onset of ejection for lowest and highest elastance curves).

should be compared with the corresponding $E(t)$ curves constructed using the conventional relationship $E(t) = P(t)/[V(t) - V_d]$ (Fig. 2*B*). Flow-related pressure reductions in $P(t)$ cause corresponding reductions in the derived $E(t)$ curves. Since these reductions depend on the magnitude and timing of flow, they vary with alterations in loading conditions. The resulting $E(t)$ curves thus exhibited considerably more load dependence than $E^*(t)$ in the rising phase of the curves during which ejection is taking place. These effects are easily appreciated in Fig. 2*C* where $E(t)$ curves are compared with the average curve of $E^*(t)$ from the data in Fig. 2*A* (for this comparison, $E(t)$ curves were calculated using V_d^*). The $E(t)$ curves superimpose on the $E^*(t)$ curve until ejection begins (see arrows in Fig. 2*C*), at which time a distinct change in curve contour is noted. The $E(t)$ curves then begin to fall below the $E^*(t)$ curve due to the flow-related pressure reductions associated with ejection.

The $E^*(t)$ curves constructed from all conditions for each heart were pooled and an average curve for each heart obtained. Each average curve was then compared with the normalized curve of ventricular elastance previously published by Suga and Sagawa (23). By introducing the two scaling values E^*_{max} and t^*_{max}, defined as the magnitude and time of maximal $E^*(t)$, respectively, the normalized curve was able to faithfully reproduce each of these average measured curves. Each ventricle could thus be characterized by the normalized curve in conjunction with only three variables: E^*_{max}, t^*_{max}, and V_d^*.

Loading system impulse response. Conceptually, the impulse response is the pressure that would result from a very narrow flow impulse injected at the aortic root. It describes both the instantaneous pressure coincident with the flow pulse and subsequent pressures maintained transiently after the pulse of flow has subsided. To obtain the vascular impulse response function, we used the method previously described by Laxminarayan et al. (10, 19) involving inverse Fourier transformation of the discrete impedance spectrum.

For each ejecting beat analyzed, the simulated aortic pressure and measured ventricular outflow were subjected to Fourier series analysis. Division of pressure moduli by flow moduli and subtraction of respective phases yields a discrete impedance spectrum. Inverse Fourier transformation of this discrete impedance spectrum yields the system impulse response function. This form of the impulse response describes the pressure that would be developed by a series of unit-flow impulses (very narrow flow pulses of unit value) repeating at intervals corresponding to the heart rate. As such, it is termed the impulse train response and will be denoted as ITR (further background information on impulse response methods is presented in the APPENDIX). An example of an ITR for the described loading system is shown by the dashed line in Fig. 3*A*. Digital filtering may be employed to smooth out artifactual oscillations appearing in the ITR, which result from high-frequency truncation (see APPENDIX). This smoothed ITR is shown by the solid line in Fig. 3*A*.

This derived ITR is subjected to two analytical modifications to facilitate the process of coupling this impulse response function with ventricular elastance. These modifications are used to adjust for the effects of missing information in the discrete impedance spectrum.

The first modification compensates for the lack of impedance information beyond the highest frequency of

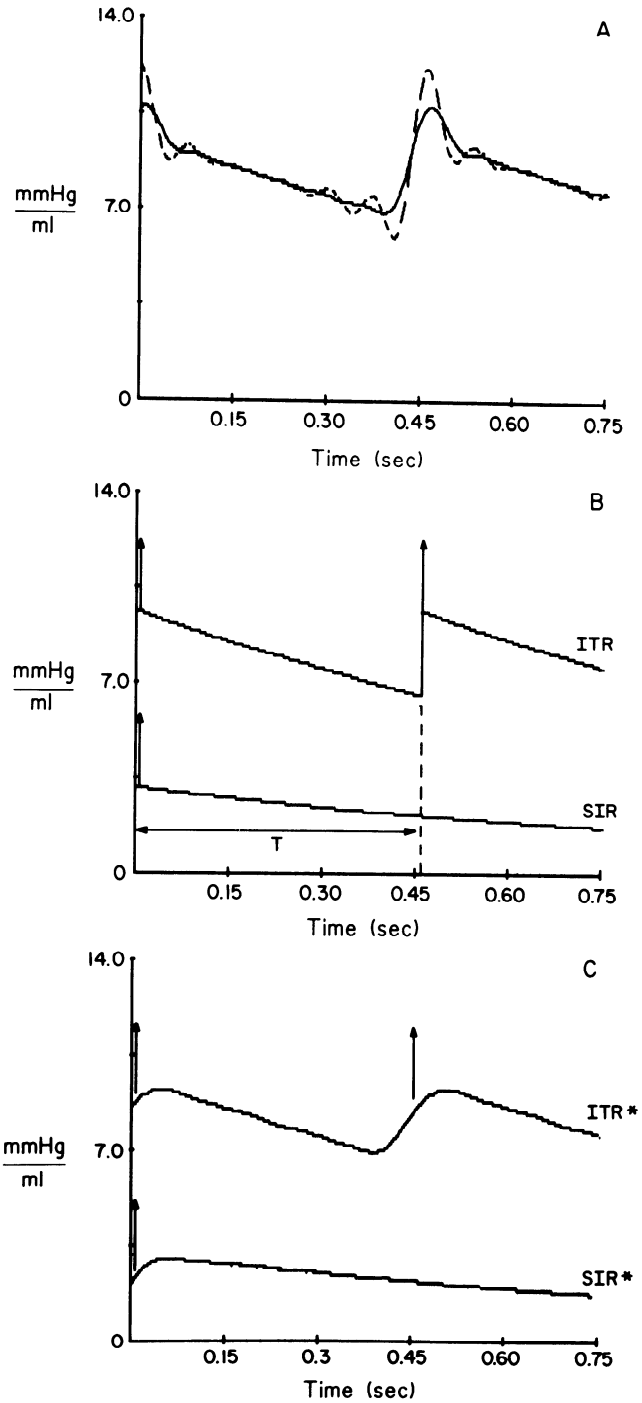

FIG. 3. Impulse response functions. *A*: impulse train response (ITR) derived by inverse Fourier transformation of loading system impedance measurements. Both filtered (*solid line*) and unfiltered (*dashed line*) forms are shown. *B*: ideal impulse response functions for a three-element Windkessel loading system. Both single (SIR) and train (ITR) responses are shown. *Vertical arrow* represents ideal impulse corresponding to series resistance property R_c. *C*: modifications made to derived ITR of *A*. ITR* is derived loading system ITR after replacing broad-based R_c peaks with an equivalent ideal impulse. SIR* represents calculated single-impulse response.

reliable measurement (the cutoff frequency). This high frequency truncation distorts the representation of any impedance properties having significant magnitude above the cutoff frequency. For the three-element Windkessel, the high-frequency impedance tends toward a constant modulus (equal to the value of the series resistance R_c) with a phase shift of zero. This high-frequency impedance pattern describes a series resistance property. The ideal impedance representation of a series resistance property is a spectrum with constant modulus that extends to infinite frequency. The ideal impulse response representation of a series resistance property has the form of an impulse (i.e., a very narrow peak of area equal to its resistance value and having a width less than or equal to the sampling interval). This is illustrated diagramatically by the arrows in Fig. 3*B*, which depicts the theoretical ideal impulse response functions for a three-element Windkessel.

The impulse response representation of this series resistance property in the derived ITR of Fig. 3*A* is the broad initial peak in the ITR function. Although this initial peak in the derived ITR retains the appropriate area (1), it is of a much greater width than its idealized representation (Fig. 3*B*) because of the effects of high-frequency truncation. This increased width, which is equal to the period of the highest harmonic, limits the minimum interval between sequential steps in the coupling process. The pressure associated with a series resistance is directly proportional to instantaneous flow, and hence the area of this peak (equal to its resistance value) should be represented within one timing step. One approach to this problem is to calculate the value of this series resistance property and then replace its broad-based (frequency-limited) representation in the derived ITR by an appropriate idealized representation of its effects (see APPENDIX for details). This is shown graphically in Fig. 3*C* by the arrows representing an idealized impulse. The value of this series resistance property may be determined by averaging the value of the higher harmonics in the impedance spectrum, similar to the standard practive for determining characteristic impedance in vivo. When this approach is used, the timing interval for successive steps in the coupling process is reduced to correspond to the original signal sampling rate (200 Hz).

The second modification compensates for the lack of impedance information between harmonics of the heart rate. Inverse transformation of an impedance spectrum measured only at multiples of a fundamental frequency (e.g., the heart rate) yields the steady-state response to a train (i.e., periodically repeating series) of impulses occurring at the heart rate. For sequential convolutional analysis it is more desirable to have the response to a single impulse. Thus this modification extrapolates from the known response produced by a train of impulses to estimate the response produced by a single impulse.

Figure 3*B* compares the theoretical impulse response functions for a three-element Windkessel produced by a single impulse and by a train of impulses (steady-state response). Note that ITR never returns to the base line, whereas the single response (SIR) follows an exponential decay to zero. This is because each successive flow impulse is input into the system before the system response from the prior impulses has time to complete its course (i.e., decay to zero). The resulting "elevation" of the train response relative to the single response is a function of the latter portion of the single response that occurs following the time T (corresponding to the repetition interval of the train response).

If the general behavior of the latter portion of the single response is known, the single response may be approximated from the train response. For the three-element Windkessel loading system used here, this latter part of the single response may be modeled by a first-order exponential decay. The time constant for this decay may be calculated from the latter portion of the train response or, alternatively, from the diastolic pressure decay. The single impulse response may then be approximated from the train response on the basis of known analytical equations describing the difference between the single and train response for a first-order exponential system (see APPENDIX for further details). This step is also illustrated in Fig. 3*C* for some example data obtained from these isolated heart experiments.

Coupling of ventricular and arterial properties. To obtain a simultaneous solution describing the coupling between the ventricle and arterial loading system, the method of sequential convolution is employed. Conceptually, this involves describing the pressures developed at the aortic root as consisting of two parts. The first component is pressure that is due to all prior flow into the arterial system. For the three-element Windkessel system, this pressure is simply due to the parallel resistance-compliance property; for the real arterial system this would include pressures due to the vascular Windkessel as well as the effects of finite wave velocity and discrete reflections. The second component is that pressure generated by flow during the present instant. $E^*(t)$ describes how the ventricle interacts with these developed pressures in terms of resultant changes in systolic ventricular volumes.

In analytical terms, this method involves sequential calculation of ventricular pressure $[P(t_i)]$, ventricular volume $[V(t_i)]$, flow $[F(t_i)]$, and arterial pressure $[P_A(t_i)]$, assuming values for the preceding time point (time = t_{i-1}) are known. The current value of time in the calculation process is t_i, and Δt is the timing interval between successive calculations.

$P_A(t)$ is determined by convolving the arterial system impulse response $SIR(t)$ with $F(t)$. At time = t_i, this convolution is of the form

$$P_A(t_i) = \int_{u=0}^{u=\infty} SIR(u)\ F(t_i - u)\ du \qquad (7)$$

where u is the convolution variable that accounts for the history of flow. This integral may be divided into two parts based on the value of u. The first part, for all values of u between Δt and $+\infty$, describes pressure due to the prior history of flow [i.e., all $F(t)$ up to time = t_{i-1}]. The second part, for $u = 0$ to Δt, relates pressure and flow over the current time interval between t_{i-1} and t_i. Since flow up until time = t_{i-1} is known, the first part of the

integral may be solved directly. *Equation 7* may then be rewritten as

$$P_A(t_i) = B_i + \int_{u=0}^{u=\Delta t} SIR(u)\ F(t_i - u)\ du \qquad (8)$$

where B_i is the integral of *Eq. 7* for $u = \Delta t$ to $+\infty$ and is thus a known value. To incorporate ventricular function into this formulation, $F(t)$ (for small Δt) may be expressed in terms of ventricular volume. The average flow between time = t_{i-1} and t_i is given by

$$F_{avg} = [V(t_{i-1}) - V(t_i)]/(\Delta t) \qquad (9)$$

From this relationship and the known value for $F(t_{i-1})$ we can describe $F(t_i)$ as a function of $V(t_i)$. When we use this relationship to make the appropriate substitutions in *Eq. 8* and after we perform the indicated numerical integration, the result may be expressed as a linear equation in the pressure-volume plane

$$P_A(t_i) = B_i - [m \times V(t_i)] \qquad (10)$$

where m is a constant derived from the integral term in *Eq. 8* (see APPENDIX). This equation is expressed by the line labeled P_A in Fig. 4. For purposes of explanation, this equation may be expanded by adding and subtracting $[m \times V(t_{i-1})]$ to the right side of the equation resulting in

$$P_A(t_i) = \{B_i - [m \times V(t_{i-1})]\} + \{m \times [V(t_{i-1}) - V(t_i)]\} \qquad (11)$$

In this expanded equation, the first term in brackets gives the pressure that is due to all prior flow into the arterial system; i.e., if there were no additional flow between t_i and t_{i-1}, $P_A(t_i)$ would be equal to this term alone. This term will vary in successive calculations depending on the prior history of flow. In Fig. 4, this term is represented by the heavy dot. For any flow that does occur in this time interval [i.e., $V(t_i) < V(t_{i-1})$], P_A will increase from this point according to the slope m appearing in the second bracketed term. The slope m is a constant related to the initial value of $SIR(t)$, (which includes the effects of any series resistance properties; see APPENDIX), and does not vary between calculations. When multiplied by the change in ventricular volume, m describes the pressure generated by flow during the present instant between t_{i-1} and t_i.

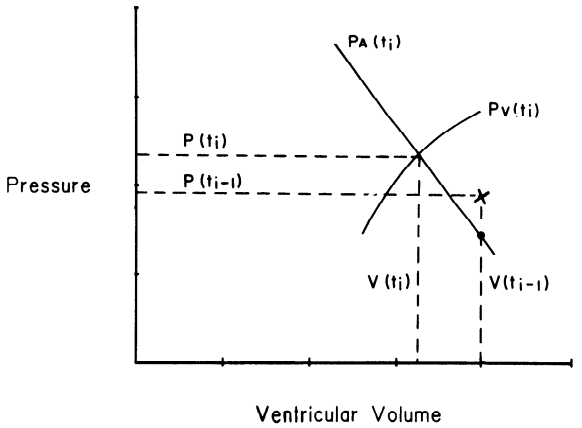

FIG. 4. Graphic analysis of calculations involved in sequential convolution. "x," Represents pressure and volume calculated from preceding step of convolution at time = t_{i-1}. *Line* labeled $P_A(t_i)$ depicts arterial pressure at time = t_i as a function of ventricular volume at time = t_i. *Heavy dot* is pressure that would occur if no flow occurred between t_{i-1} and t_i. $P_V(t_i)$ depicts ventricular pressure as a function of ventricular volume at time = t_i. Intersection of P_A and P_V represents simultaneous solution predicting both pressures and volume at time = t_i.

To describe ventricular pressure $P(t)$, we can rearrange *Eq. 6* as

$$P(t_i) = E^*(t_i)[V(t_i) - V_d^*]/1 - [F(t_i) \times RF] \qquad (12)$$

When we used the methods previously described, E^*_{max}, t^*_{max}, and V_d^* were determined for each heart. $E^*(t_i)$ is then obtained from the normalized curve of ventricular elastance (same for all hearts) scaled by the factors E^*_{max} and t^*_{max}. RF is assumed constant for all hearts. After making a similar substitution for $F(t_i)$ (based on *Eq. 9*), the only unknowns in *Eq. 12* (for time = t_i) are $P(t_i)$ and $V(t_i)$. As shown in Fig. 4, the relation between these describes a curve in the pressure-volume plane that is slightly concave toward the volume axis.

Equations 10 and *12* thus contain three unknown variables: $P(t_i)$, $P_A(t_i)$, and $V(t_i)$. If we add the constraint that during ejection $P_A(t_i)$ is equal to $P(t_i)$, we have three equations for three unknowns and can solve simultaneously for all three unknowns. As depicted in Fig. 4, the intersection of the two lines describing $P_A(t_i)$ and $P(t_i)$ as a function of $V(t_i)$ represents this solution. After determining these values, the present t_i becomes t_{i-1}, and the value of t_i is incremented by Δt. The above calculation cycle is now repeated to determine the values of $V(t_i)$, $P_A(t_i)$, and $P(t_i)$ for the new t_i. During periods where $F(t) = 0$ [i.e., $P(t) < P_A(t)$], the two systems do not interact and can be solved separately. For modeling steady-state conditions, as was done in the present study, the computer was made to cycle until the difference between arterial diastolic pressures at the beginning and end of a simulated cardiac cycle became <1 mmHg.

RESULTS

We compared the pressures, volumes, and flows predicted by the coupling method described above to the values actually measured in four isolated canine hearts. In Figs. 5–7, the solid lines depict the predicted variables and the dotted lines show the corresponding measured values. Each panel in these figures illustrates results obtained from a single heart following variable manipulations in loading conditions (during periods of presumed constant contractility). The same $E^*(t)$ model parameter values (E^*_{max}, t^*_{max}, V_d^*) were used for all of the predicted curves in each panel.

Figure 5 illustrates the pressure-volume loops for *ventricles 1* and *2* obtained over a moderate range of end-diastolic volumes (25.3–37.3 ml) and a wide range of R_p values (R_p = 1–8 mmHg·s/ml). Note that peak pressure and stroke volumes varied more than twofold during these tested loading conditions. Ejection fraction also varied considerably, ranging from 22 to 54%. Despite these large changes, the predicted ventricular pressure-volume loops closely matched the loops constructed from

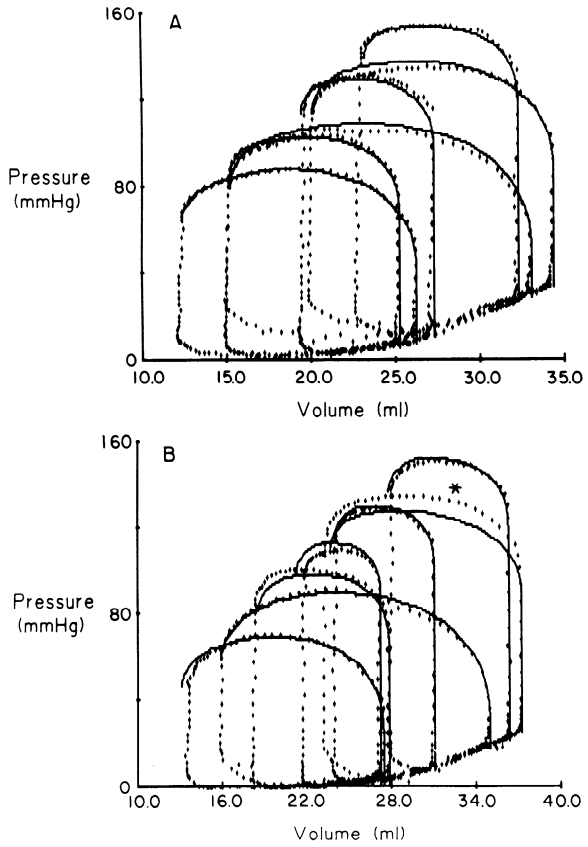

FIG. 5. Predicted (*solid lines*) and observed (*dotted lines*) pressure-volume loops for *ventricles 1* (*A*) and *2* (*B*) during changes in end-diastolic volume and R_p (range of R_p: 1–8 mmHg·s·ml^{-1}).

TABLE 1. *Differences between predicted and observed values*

Ventricle	No. Different Loads	Peak Flow, ml/s	Peak Pressure, mmHg	Stroke Volume, ml	E^*_{max}, mmHg/ml
1	6	2.5±2.8	−0.3±2.1	0.1±1.3	6.4±0.1
		(3.2±3.3)	(−0.3±2.1)	(0.7±1.4)	
2	7	0.7±4.2	0.7±3.4	0.0±0.3	6.8±0.3
		(0.9±3.3)	(0.6±2.7)	(−0.7±3.6)	
3	9	2.7±3.1	−0.2±3.5	0.0±0.3	4.1±0.15
		(3.1±3.5)	(−0.2±2.9)	(0.0±2.7)	
4	6	6.2±4.6	−1.7±3.2	0.1±0.2	5.8±0.1
		(4.0±2.7)	(−0.8±1.5)	(0.3±1.1)	

Values are means ± SD for the differences given between observed values and model predictions for peak flow, peak pressure, and stroke volume. Nos. in parentheses are differences expressed as a percentage of observed values. The last column gives the mean and standard deviation of the maximal elastance (E^*_{max}) values measured for each ventricle.

the measured data. The mean differences between predicted and observed peak pressure, peak flow, and stroke volume are given in Table 1 for each ventricle.

Figure 6 depicts sample results for *ventricles 3* and *4* during a combination of changes in C, R_c, and R_p. These very large changes in R_c and C produces marked alterations in the contours of the pressure-volume loops. Large values of R_c resulted in large systolic pulse pressures, but low end-ejection pressures, such that ejection continued somewhat past the time of maximal ventricular elastance. Large values of C resulted in a similar prolongation of ejection but with much lesser changes in systolic

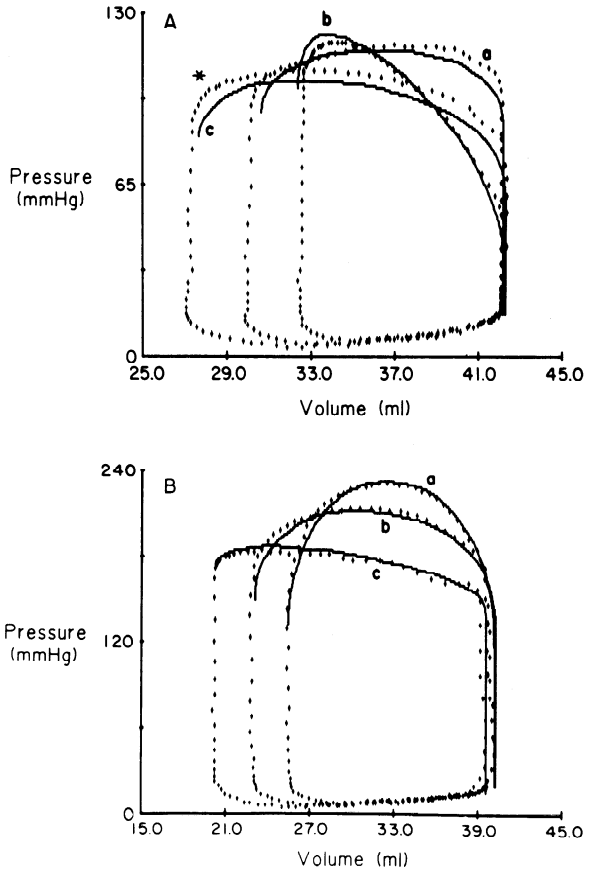

FIG. 6. Predicted (*solid lines*) and observed (*dotted lines*) pressure-volume loops for *ventricles 3* (*A*) and *4* (*B*) during changes in R_p (mmHg·s·ml^{-1}), R_c (mmHg·s·ml^{-1}), and C (ml/mmHg). Loading conditions were as follows. *A, curve a:* C, 1.5; R_c, 0.3; R_p, 3.7; *curve b:* C, 0.1; R_c, 0.4; R_p, 3.7; *curve c:* C, 0.3; R_c, 0.3; R_p, 2.4. *B, curve a:* C, 0.3; R_c, 0.9; R_p, 3.7; *curve b:* C, 0.3; R_c, 0.5; R_p, 3.7; *curve c:* C, 0.3; R_c, 0.1; R_p, 3.7. See ABBREVIATIONS for definitions.

pressure. Small values of C produced increased systolic and diastolic pulse pressures with relatively high end-ejection pressures. Even with these changing ejection patterns, the predicted curves still closely paralleled the measured curves.

Note that close agreement of these pressure-volume loops requires that the time courses of both pressure and flow be accurately predicted. Typical comparisons between measured and predicted pressures and flows, as a function of time, are shown in Fig. 7. Both pressure and flow waveform are well reproduced, with only small deviations in contours.

The curves marked by asterisks in Figs. 5*B* (*ventricle 2*) and 6*A* (*ventricle 3*) represent the largest differences obtained between predicted and observed results. These larger differences reflected slightly higher variability in the calculated $E^*(t)$ curves for these hearts (see Table 1). For example, the starred curve in Fig. 6*A* corresponds to the highest $E^*(t)$ curve shown in Fig. 2*A*, which exceeded the average $E^*(t)$ curve by 6%. As explained above, all of the simulations for a given heart used a single set of elastance parameters based on the average $E^*(t)$ curve for that heart. The model elastance for this simulation was thus less than the measured $E^*(t)$ by 6% and resulted in slightly lower predicted pressures and stroke volume. Even these pressure-volume differences

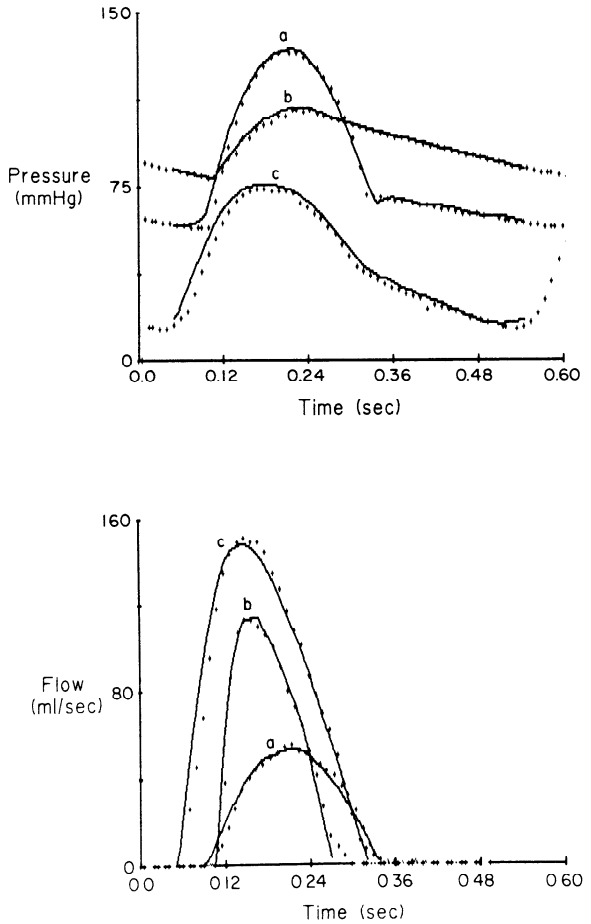

FIG. 7. Example comparisons between predicted (*solid lines*) and observed (*dotted lines*) aortic pressure and flow as a function of time. Loading conditions were as follows with C in ml/mmHg and R_c and R_p in mmHg·s·ml^{-1}. *Curve a:* C, 0.4; R_c, 1.4; R_p, 3.8; *curve b:* C, 0.3; R_c, 0.1; R_p, 3.7; *curve c:* C, 0.3; R_c, 0.3; R_p, 0.6. See ABBREVIATIONS for definitions.

are still relatively small considering that ejection fraction, stroke volume, and peak pressure varied in excess of twofold during the tested loading conditions.

DISCUSSION

The primary goal of the present study is to describe an analytical method by which the interaction between ventricular mechanical function and complex vascular properties may be studied. This method enabled accurate prediction of flow and pressures in isolated canine hearts ejecting into a simulated arterial loading system. Two steps were involved in this process. The first step involved developing independent descriptions of ventricular and vascular properties, and the second step involved coupling these independent descriptions by sequential convolution. Earlier investigators have used other means by which this first step might be accomplished. However, the use of sequential convolution to couple these independent descriptions has not been previously reported.

Although impedance studies are useful in describing complex vascular properties, they are based on the relationship between sinusoidal oscillations (frequency harmonics) of pressure and flow in the arteries. Unfortunately, such descriptions relating pressure and flow as a function of frequency are difficult to couple with descriptions of ventricular mechanical properties expressed as a function of time (11). For coupling, compatible descriptions must be used for both ventricle and arteries. Since the frequency-based approach is not readily applicable to describe ventricular function (9), we sought to use the alternative of describing arterial properties as a function of time using impulse response techniques.

In this initial study the arterial system used was limited to a simple Windkessel model. Such a model does not reproduce some of the more complex phenomenon that occur in vivo, such as the effects of finite wave velocity and vascular reflections. Resultant differences in the impedance properties of the arterial system compared with that of the three-element Windkessel have long been recognized, and corresponding differences in the impulse response functions of the two systems have recently been described (19). However, the importance of these differences in terms of their effects on ventricular loading remains debated.

Although it has not yet been thoroughly tested, the sequential convolution method should also be applicable with the more complex impulse response functions of the in vivo arterial system. This ability highlights the strength of this method. Figure 8 gives an example of this potential use of sequential convolution with more complex arterial behavior. We coupled a ventricular model with an impulse response function derived from in vivo canine aortic root pressure and flow measure-

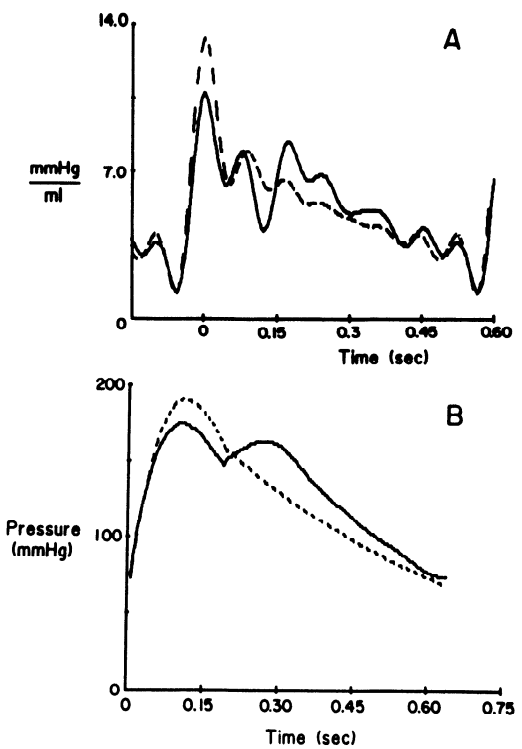

FIG. 8. Example results from using sequential convolution to couple a ventricular model with a vascular impulse response function derived from canine aortic root pressure and flow measurements. *A*: unfiltered impulse train response functions derived from measured data (*solid line*) and from a corresponding 3-element Windkessel model (*dashed line*). *B*: simulated aortic pressures produced by coupling these impulse response functions to a typical ventricular model.

ments. The unsmoothed vascular impulse train response used in this analysis is shown in Fig. 8*A* (solid line). For comparison, the ITR derived from a corresponding three-element Windkessel model is also shown (dashed line). The Windkessel parameters were set to match the in vivo arterial impedance as follows: R_c equal to characteristic impedance, R_p equal to total systemic resistance minus R_c, and C determined from R_p and the time constant of the latter part of the diastolic pressure decay. The simulated aortic pressures resulting from coupling these impulse response functions to a typical ventricular model are shown in Fig. 8*B*. Note that the pressure waveforms differ in a manner analogous to the differences observed in the ITRs. In this example, using the vascular ITR as compared with the Windkessel ITR resulted in an increase of pressure during diastole and a reduction of pressure during systole. Correspondingly, there was ~5% increase in stroke volume.

As in many cardiovascular studies, the experimental data on which we based our analysis was obtained at a fixed physiological heart rate. The calculated impedance spectrum thus contained information only at frequencies that were multiples of the heart rate. As a result, the derived impulse response function was not that produced by a single impulse; rather it was the response produced by a train of impulses. There are several approaches for handling this problem. The first would be to limit any subsequent use of the impulse response function to steady-state analyses at the same heart rate as the original data. This was the approach used by Piene (13) in a previous study. Another approach is to supplement the limited impedance information by making an assumption about the form of the single impulse response. We chose this method in our current study and assumed that the latter part of the single impulse response could be modeled as first-order exponential decay. This assumption allows us to estimate the single impulse response from our limited data (see APPENDIX). Once estimated, the single response can be used with sequential convolution to predict arterial behavior at any heart rate. This is obviously a reasonable approach for our simple Windkessel model and it may also be valid for in vivo vascular studies, but this latter application will require further study. It should be noted that this approach will still give valid results for steady-state analyses at the original heart rate (as with the first approach) even if the underlying assumption about the form of the latter part of the single response is invalid. Errors in this underlying assumption will, however, result in errors in non-steady-state analyses or analyses at other than the original heart rate.

The best approach for deriving the single impulse response would be to obtain the missing frequency information by varying cardiac rhythm (12). The repetition period of the derived ITR is equal to the inverse of the frequency interval between known values in the impedance spectrum. By lessening this interval and hence lengthening the period of each cycle in the ITR, a given cycle of the ITR will (in theory) approach the response to a single impulse. Other methods of obtaining the vascular impulse response function by numerical deconvolution in the time domain have also been investigated (15, 16) and may provide yet another means to obtain the single impulse response function.

An inherent problem in using the impulse response description involves accounting for the effects of the high-frequency components of impedance. For the Windkessel model used here, as well as for large vessels in vivo (29), these high-frequency components tend toward a constant modulus with zero phase shift (i.e., exhibit properties characteristic of a series resistance). This impedance pattern would ideally give rise to a very narrow spike in the impulse response function. However, with real data limited by a certain cut-off frequency, this spike appears in the derived ITR as a broadened peak with smaller oscillations to either side (see APPENDIX). The increased width of this series resistance peak limits the minimum interval between sequential steps in the coupling process. As explained in MATERIALS AND METHODS (with further details in the APPENDIX), we approached this problem by extracting the series resistance component from the original impedance spectrum and then later introducing a series resistance directly in the convolution equations.

Comparisons With Previous Studies

Our approach to ventricular-vascular coupling using the impulse response function with sequential convolution may be contrasted to that in a prior study by Piene (13). The method he described used the impulse train response of the simulated vascular loading system with a nonsequential iterative alogarithm that searched globally through all of systole for the interval where the predicted error was largest. Flow in this interval was adjusted, and then the global error search process repeated again until the best fit was obtained. Limitations of this approach include *1*) only steady-state conditions at the observed heart rates may be modeled; and *2*) it is more difficult to incorporate factors that may affect ventricular performance as ejection proceeds in a time-sequential manner (e.g., ventricular internal resistance, possible inertial terms). The author also commented that the described method sometimes "broke down" when marked reflections were evident in the impulse response, producing nonconverging oscillations in calculated flow. The advantages of the present method include *1*) calculations proceed in a time-sequential manner without reliance on best-fit algorithms; *2*) both non-steady-state conditions and conditions at other than the observed heart rates may be modeled; and *3*) the concept of aortic root pressures being the sum of the effects of instantaneous flow plus prior flow is more readily apparent.

Prior work by Sunagawa et al. (28) has employed the concept of ventricular and arterial elastance to analyze "ventriculoarterial interactions." They derived a set of analytical equations predicting stroke volume from a given set of ventricular and vascular parameters. Although it provided insights into the relative importance of different parameters, this study made no attempt to predict the complete time course of pressure and flow throughout the cardiac cycle. The derived equations were also limited to three-element Windkessel descriptions of

vascular properties.

Studies by at least three other groups (3, 5, 7) have used sets of simultaneous differential equations to model the effects of ventricular-vascular interactions. These studies have utilized iterative parameter estimation techniques to optimize sets of ventricular and vascular parameters contained in a predefined set of differential equations. Thus the techniques of vascular characterization were inherently model dependent. Use of the vascular impulse response function offers the potential for a more model-independent method of characterizing the influence of vascular properties on ventricular loading. Furthermore, none of these studies used a single set of ventricular parameter values to predict pressure and flow over a wide range of loading conditions, as was done in the present study.

Successful modeling of ventricular-vascular interactions requires a load-independent description of ventricular pump function. Several previous investigators have used the conventional definition of $E(t)$ without an "internal resistance" for this purpose (21, 22, 26, 28). For example, Sunagawa and co-workers (28) have demonstrated that stroke volumes and mean pressures could be accurately predicted by coupling ventricular $E(t)$ with the elastance of a three-element Windkessel load. Our preliminary studies indicated, however, that when attempting to predict instantaneous pressure and flow, ventricular resistance effects were capable of causing significant error. A similar conclusion was reached by Campbell et al. (4) in their studies predicting instantaneous flow from the right ventricle and by Shroff et al. (17) in their theoretical analysis of the effects of ventricular resistance on pulsatile pressure. Inclusion of a ventricular internal resistance in our analytical methods using the equations given for $E^*(t)$ substantially improved model predictions. This improvement relates to the more uniform contour of the rising phase of the $E^*(t)$ curves during which ejection occurs. By accounting for the effects of flow-related pressure reduction, the $E^*(t)$ curves exhibited considerably less load dependence than the corresponding $E(t)$ curves. The small variations that were observed in the $E^*(t)$ curves did not appear to be systematically related to loading system conditions. They may relate to small fluctuations in contractility over time or, alternatively, to factors affecting ventricular pressure that are not accounted for by these methods.

For these initial studies an assumed average value of 0.0015 s/ml was used for the resistance factor RF. Work by other investigators has suggested that the value of RF is independent of contractility (17) but may vary between hearts. The range of published values is 0.0011–0.0023 s/ml with average values between 0.0014 and 0.0015 s/ml (17, 18, 24). Since the effects of internal resistance are relatively small in magnitude, small variations in actual RF values from our assumed value would result in minimal error (probably within the range of measurement error). Large deviations of RF from the assumed value should have produced a recognizable pattern of errors. Had this been observed, an iterative algorithm could have been used to determine an RF value for each heart.

Conclusion

These studies have demonstrated the ability of the above methods to accurately predict ventricular-vascular interactions for the isolated canine left ventricle ejecting into a simulated arterial system. Further investigations are needed to assess both the applicability and limitations of these methods for in vivo studies. The described technique of sequential convolution to couple independent descriptions of ventricular and vascular properties may also be useful with alternate methods of describing ventricular performance and/or determining the vascular impulse response function.

APPENDIX

General Definition of Impulse Response

The ideal unit impulse response of any linear time-invariant system is the output produced by the input of an ideal unit impulse. An ideal unit impulse is an infinitely narrow pulse of unit area (e.g., if the width is w, then the height is 1/w; this is illustrated diagrammatically by a thin arrow). The impulse train response of a system is defined as the steady-state output that would result from the input of a periodic series of ideal impulses. Impulse response functions for a three-element Windkessel model are shown in Fig. A1.*a*. Once the impulse response of a system is known, the output for any given input may be predicted by the process of convolution. This involves describing the input as the summation of a group of unit impulses and then calculating the output from the summation of a corresponding group of unit impulse responses.

Differences Between Derived and Ideal Impulse Train Response

As previously described by Laxminarayan et al. (10), the impulse train response (ITR) of the vascular system may be derived by inverse Fourier transformation of the discrete impedance spectrum (i.e., a spectrum determined by Fourier series methods that is limited to discrete values at frequencies corresponding to integer multiples of the heart rate). Such a derived ITR differs from the ideal ITR of Fig. A1.*a* because only a limited number of higher frequency harmonics are known. This restricts the impedance frequency range used in the inverse transformation and introduces a type of low pass filtering termed high frequency truncation (Fig. A1.*b*). Conceptually, this has the effect of changing our idealized input flow impulses from infinitely narrow spikes to broader-based flow pulses $I(t)$ of the form shown in Fig. A1.*b*, and described by the equation

$$I(t) = 2Fc\ [\sin(2Fc \times \pi \times t)]/(2Fc \times \pi \times t) \qquad (1A)$$

where 2Fc is twice the frequency of the highest harmonic, and π is the numeric constant 3.1416. The derived ITR represents the output produced by the input of a train of such modified flow pulses. These flow pulses differ from the idealized impulses in two ways: *1*) the main flow pulse is much broader than an impulse (the width of the main flow pulse is equal to the period of the highest harmonic in the impedance spectra), and *2*) smaller rapidly decaying oscillations (side lobes) appear on each side of the main flow pulse. The derived ITR correspondingly differs from the ideal ITR in two ways. First, any abrupt changes in magnitude in the ideal ITR are less sharply defined in the derived ITR. For example, note that the initial spike in the ideal ITR appears as a broader rounded peak in the derived ITR. Second, artifactual oscillations now appear in the derived

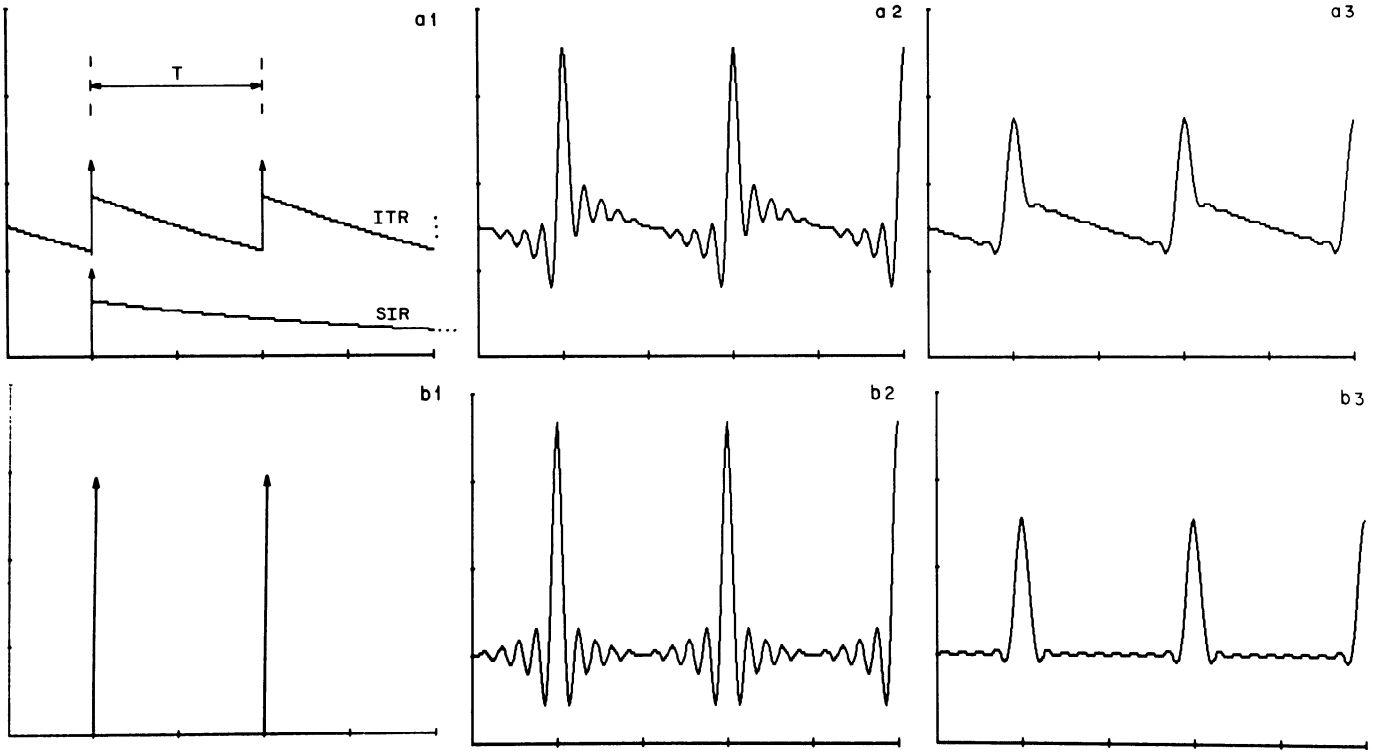

FIG. A1. *Panel a1*: ideal single (SIR) and train (ITR) impulse response functions for a three-element Windkessel model composed of a series resistance R_c and parallel resistance-capacitance combination R_p-C. SIR represents output produced by input of a single ideal impulse. ITR is output produced by periodic series of ideal impulses shown in *b1*. Panel *a2*: derived ITR corresponding to ideal ITR of *a1*. This ITR would be produced by input of modified flow pulses shown in *b2* (see text for explanation). *Panels a3* and *b3* show effects of digital filtering designed to smooth out artifactual oscillations resulting from high-frequency truncation.

ITR, reflecting the smaller side oscillations in the modified flow pulses. These oscillations may be smoothed out by using an appropriate digital filter. As shown in Figs. A1.*a3* and *b3*, however, this process will further broaden the effective input flow pulses and cause more distortion of the initial peak in the derived ITR.

Accounting for Effects of Series Resistance Properties

The initial peak in the ITR is due to the series resistance property R_c of the three-element Windkessel (analogous to characteristic impedance in vivo). As depicted in Fig. A1.*a*, the ideal impulse response of a series resistance is an infinitely narrow impulse of the same form as the input impulse (but having an area equal to its resistance value). In contrast, the derived impulse response of a series resistance is much wider, having a form similar to that of the modified input flow pulse $I(t)$ (Fig. A1.*b*). Removal of this broad-based peak in the ITR may be done by subtracting the impedance representation of this series resistance property (to be denoted by R_s) from the impedance of the total system (using complex numbers to account for phase and magnitude relationships). The impedance spectrum of this peak is a series of harmonic values with modulus equal to the resistance value R_s (determined by averaging the high frequency impedance moduli) and a phase of zero. Subtraction of this series resistance spectrum from total system impedance yields a residual impedance spectrum that describes the impedance of the loading system minus the effects of the subtracted series resistance. Inverse transformation of this residual impedance spectrum thus yields the system impulse train response minus the effects of the subtracted series resistance. Note that even if the impedance spectrum does contain some additional high frequency components that are not accounted for by a series resistance, these additional components will still remain in the residual impedance spectrum. In the ensuing discussion, an asterisk will be used to denote when an impulse response has been modified in this manner (e.g., ITR*). An example ITR* was shown in Fig. 3*C*. During sequential convolution, the combination of this type of modified impulse response function plus a numerical representation of the subtracted series resistance is equivalent to the original impulse response function (over the range of known impedance values). As described below, this numerical representation of the effects of this subtracted series resistance is simply a constant (equal to the determined series resistance value) multipled by instantaneous flow.

Approximating Single Response From Train Response

Inverse Fourier transformation of a discrete impedance spectra yields the impulse train response rather than the single response. This is because discrete sampling in the frequency domain produces a periodic function in the time domain (2). The general behavior of the single response beyond the repetition period T determines how the single response differs from the train response. For a three-element Windkessel, this general behavior of the latter part of the impulse response may be modeled as a first-order exponential decay.

Conceptually, the steady-state train response between $t = 0$ and T is equal to the single response plus a variable offset (see Fig. A1.*a*). This offset is determined by *1*) the interval between flow impulses in the impulse train, and *2*) the latter part of the single impulse response. For a system exhibiting first-order exponential decay properties, this offset may be determined

from the following equations describing the impulse response functions for this type of system (15). Single response

$$\mathrm{SIR}_{ex}(t) = \mathrm{I} \times e^{-t/\tau} \quad (2A)$$

where τ is equal to the time constant of decay and I is equal to the extrapolated y-axis intercept at time = 0. Train response (for $t = 0$ to T)

$$\mathrm{ITR}_{ex}(t) = K \times \mathrm{SIR}_{ex}(t) \quad (3A)$$

where $K = 1/(1 - e^{-T/\tau})$. Offset of train from single response

$$\mathrm{OFFSET}_{ex}(t) = \mathrm{ITR}_{ex}(t) - \mathrm{SIR}_{ex}(t) = \mathrm{SIR}_{ex}(t) \times (K - 1) \quad (4A)$$

To approximate the single response of the loading system from the train response, we divide the single response into two portions: between $t = 0$ to T, and $t > T$. The first portion may contain additional components other than that which is described by the first-order exponential decay property of the system. For example, this initial portion for the three-element Windkessel model also contains the effects of R_c. For the intact vascular system, this initial portion would contain the effects of finite wave velocity and discrete reflections. This portion of the single response may be approximated from the train response by subtracting the variable offset (*Eq. 4A*) from the train response. For $t = 0$ to T

$$\mathrm{SIR}^*(t) = \mathrm{ITR}^*(t) - \mathrm{OFFSET}_{ex}(t) \quad (5A)$$

Note that we have used the modified form of the derived ITR in this equation (although the original derived ITR could be used, this would require extending t backward from 0 to accommodate the increased width of the R_c peak).

We have assumed that the latter portion of the single impulse response function may be modeled solely by a first-order exponential decay. The second portion of $\mathrm{SIR}^*(t)$ (for $t > T$) is thus given by substituting the determined values of I and τ into *Eq. 2A*. For $t > T$

$$\mathrm{SIR}^*(t) = \mathrm{SIR}_{ex}(t) \quad (6A)$$

This analysis assumes that *1)* the magnitude of discrete reflections in the loading system (artificial or in vivo) is insignificant outside the period T, and *2)* the major time-delaying storage properties of the system (i.e., those properties of significant duration that cause the train response not to return to base line between repetitive impulses) may be approximated by a first-order decay. These assumptions are valid for the simulated arterial loading system used in these studies. Initial results obtained using the canine vascular ITR also support the feasibility of these modeling assumptions for in vivo work but additional studies are needed.

*Convolution using SIR**

SIR in *Eq. 7* can be expressed as the combination of SIR* and the series resistance property R_s that was subtracted from the original impedance spectrum. This expanded equation has the form of

$$P_A(t_i) = [F(t_i) \times R_s] + \int_{u=0}^{u=+\infty} \mathrm{SIR}^*(u)\, F(t_i - u)\, du \quad (7A)$$

Equations 8–10 describing the sequential convolution algorithm are derived as before, and the value R_s becomes incorporated into the constant m of *Eq. 10*.

The authors thank Dr. F. C. P. Yin (Dept. of Cardiology, Johns Hopkins Medical School) for contributing the canine impedance data that were used to evaluate the feasibility of applying these techniques to studies of the in vivo vascular system.

This work was supported in part by the National Heart, Lung, and Blood Institute Research Grant R01-HL-14903 and by a Researcher Starter Grant awarded to T. Latson by the American Society of Anesthesiologists. W. Hunter was supported by Research Career Development Award HL-01232 from the National Heart, Lung, and Blood Institute.

Received 25 October 1985; accepted in final form 26 June 1986.

REFERENCES

1. BRACEWELL, R. *The Fourier Transform and Its Applications.* New York: McGraw-Hill, 1965.
2. BRIGHAM, E. O. *The Fast Fourier Transform.* Englewood Cliffs, NJ: Prentice-Hall, 1974.
3. CAMPBELL, K. B, J. A. RINGO, AND J. E. ALEXANDER. Informational analysis of left-ventricle/systemic-arterial interaction. *Ann. Biomed. Eng.* 12: 209–231, 1984.
4. CAMPBELL, K. B., J. A. RINGO, Y. WAKOO, P. A. KLAVANO, AND J. E. ALEXANDER. Internal capacitance and resistance allow prediction of right ventricle outflow. *Am. J. Physiol.* 243 (*Heart Circ. Physiol.* 12): H99–H112, 1982.
5. CLARK, J. W., R. S. LING, R. SRINIVASAN, J. S. COLE, AND R. C. PRUETT. A two-stage identification scheme for the determination of the parameters of a model of left heart and systemic circulation. *IEEE Trans. Biomed. Eng.* 27: 20–29, 1980.
6. DEMOMENT, G., AND J. HINGLAIS. Global parametric search and left ventricular identification. *Ann. Biomed. Eng.* 9: 59–74, 1981.
7. DESWYSEN, B. A. Parameter estimation of a simple model of the left ventricle and of the systemic vascular bed, with particular attention to the physical meaning of the left ventricular parameters. *IEEE Trans. Biomed. Eng.* 24: 29–38, 1977.
8. HUNTER, W. C., J. S. JANICKI, K. T. WEBER, AND A. NOORDERGRAFF. Flow-pulse response: a new method for the characterization of ventricular mechanics. *Am. J. Physiol.* 237 (*Heart Circ. Physiol.* 6): H282–H292, 1979.
9. HUNTER, W. C., AND A. NOORDERGRAAF. Can impedance characterize the heart? *J. Appl. Physiol.* 40: 250–252, 1976.
10. LAXMINARAYAN, S., P. SIPKEMA, AND N. WESTERHOF. Characterization of the arterial system in the time domain. *IEEE Trans. Biomed. Eng.* 25: 177–184, 1978.
11. MILNOR, W. R. Arterial impedance as ventricular afterload. *Circulation* 36: 565–570, 1975.
12. O'ROURKE, M. F., AND M. G. TAYLOR. Input impedance of the systemic circulation. *Circ. Res.* 20: 365–380, 1967.
13. PIENE, H. Interaction between the right heart ventricle and its arterial load: a quantitative solution. *Am. J. Physiol.* 238 (*Heart Circ. Physiol.* 7): H932–H937, 1980.
14. ROBINSON, D. A. Quantitative analysis of the control of cardiac output in the isolated left ventricle. *Circ. Res.* 17: 207–221, 1965.
15. SEGALEN, A. *Study of a New Algorithm (Constrained Adaptive Least Squares): Application to the Identification of the Properties of the Pulmonary Vascular Bed in the Dog.* (PhD thesis in French). Paris: Univ. of Paris (Orsay), 1982.
16. SEGALEN, A., D. SAINT-FELIX, G. DEMOMENT, J. L. CHEVRIER, AND BUI-MONG-HUNG. Quantitative study of pulmonary vascular bed adaptivity. In: *Proceedings of the Thirty-fourth Conference of Engineering in Medicine and Biology.* 1981.
17. SHROFF, S. G., J. S. JANICKI, AND K. T. WEBER. Evidence and quantitation of left ventricular systolic resistance. *Am. J. Physiol.* 249 (*Heart Circ. Physiol.* 18): H358–H370, 1985.
18. SHROFF, S. G., J. S. JANICKI, AND K. T. WEBER. Left ventricular systolic dynamics in terms of its chamber mechanical properties. *Am. J. Physiol.* 245 (*Heart Circ. Physiol.* 14): H110–H124, 1983.
19. SIPKEMA, P., N. WESTERHOF, AND O. S. RANDALL. The arterial system characterized in the time domain. *Cardiovasc. Res.* 14: 270–279, 1980.
20. SONNENBLICK, E. H. Force-velocity relations in mammalian heart muscle. *Am. J. Physiol.* 202: 931–939, 1962.
21. SUGA, H. Theoretical analysis of a left-ventricular pumping model based on the systolic time-varying pressure/volume ratio. *IEEE Trans. Biomed. Eng.* 18: 47–55, 1971.
22. SUGA, H., A. KITABATAKE, AND K. SAGAWA. End-systolic pressure determines stroke volume from fixed end-diastolic volume in the isolated canine left ventricle under a constant contractile state. *Circ. Res.* 44: 238–249, 1979.

23. SUGA, H., AND K. SAGAWA. Instantaneous pressure-volume relationships and their ratio in the excised supported canine left ventricle. *Circ. Res.* 35: 117–125, 1974.
24. SUGA, H., K. SAGAWA, AND L. DEMER. Determinants of instantaneous pressure in canine left ventricle. Time and volume specification. *Circ. Res.* 46: 256–263, 1980.
25. SUGA, H., K. SAGAWA, AND A. A. SHOUKAS. Local independence of the instantaneous pressure-volume ratio of the canine left ventricle and effects of epinephrine and heart rate on the ratio. *Circ. Res.* 32: 314–322, 1973.
26. SUGA, H., AND K. YAMAKOSHI. Effects of stroke volume and velocity of ejection on end-systolic pressure of canine left ventricle. End-systolic volume clamping. *Circ. Res.* 40: 445–450, 1977.
27. SUNAGAWA, K., D. BURKHOFF, K. O. LIM, AND K. SAGAWA. Impedance loading servo pump system for excised canine ventricle. *Am. J. Physiol.* 243 (*Heart Circ. Physiol.* 12): H346–H350, 1982.
28. SUNAGAWA, K., W. L. MAUGHAN, D. BURKHOFF, AND K. SAGAWA. Left ventricular interaction with arterial load studied in isolated canine ventricle. *Am. J. Physiol.* 245 (*Heart Circ. Physiol.* 14): H773–H778, 1983.
29. WESTERHOF, N., G. ELZINGA, AND P. SIPKEMA. An artificial arterial system for pumping hearts. *J. Appl. Physiol.* 31: 776–781, 1971.